EDGE ARTICLE

Formation and fine-tuning of metal–organic frameworks with carboxylic pincers for the recognition of a C$_2$H$_2$ tetramer and highly selective separation of C$_2$H$_2$/C$_2$H$_4$†

Yuefeng Duan,‡[a] Yuhang Huang,‡[a] Chongqing Wang,[a] Qian Wang,[b] Kai Ge,[a] Zhiyong Lu, [b] Huijie Wang,[a] Jingui Duan, *[a] Junfeng Bai*[b] and Wanqin Jin [a]

Highly efficient ethylene (C$_2$H$_4$) and acetylene (C$_2$H$_2$) separation is a great challenge and an important process in current industries. Herein, we finely tune a new family of 6-c metal–organic frameworks (MOFs) with crab-like carboxylic pincers for the recognition of a C$_2$H$_2$ tetramer and afford **NTU-72** with high adsorption C$_2$H$_2$/C$_2$H$_4$ selectivity (56–441, 298 K) as well as unprecedented recovery of both highly pure C$_2$H$_4$ (99.95%) and C$_2$H$_2$ (99.36%). Furthermore, the effective binding of a C$_2$H$_2$ tetramer by **NTU-72**'s carboxylic pincers has been revealed by gas-loaded crystallography and Raman spectral studies. Our work provides a novel approach for the selective binding of a small molecular cluster for designing high-performance MOFs.

Introduction

As components of cracked gas, C$_2$H$_4$ and C$_2$H$_2$ are important raw materials for the synthesis of various organic compounds such as polyethylene, α-ethynyl alcohols, and acrylic acid derivatives.[1–3] The preparation of these value-added products generally requires a high-purity feed gas. In industry, pure C$_2$H$_4$ is realized by solvent absorption or selective catalytic hydrogenation from cracked gas, which are energy consuming processes.[4,5] Meanwhile, the recovery of high-purity C$_2$H$_2$ is generally ignored in this process.

Adsorptive separation using porous materials is more environmentally friendly and energy efficient, and is regarded as a promising future separation technology.[6–11] As emerging porous materials, metal–organic frameworks (MOFs), derived from the self-assembly of organic ligands and inorganic nodes, demonstrate great opportunities to distinguish these two kinds of gas molecules by dedicated framework regulations, despite them having nearly identical molecular dimensions and physical properties.[12–15] For example, the MOF materials SIFSIX-Cu-i[7]

and NKMOF-1-Ni[16] exhibit minimal trade-off between adsorption capacity and selectivity, while the flexible UTSA-300 (ref. 17) demonstrates gating separation of these mixtures. However, they all produce lower purity C$_2$H$_2$ during desorption, even for the sieving materials, as both C$_2$H$_2$ and C$_2$H$_4$ molecules can interact with strong binding sites, or the more or less flexibility of the sieving frameworks allows a certain amount of co-adsorption.[18,19]

MOFs with free carboxylic acids might be potential light hydrocarbon separation materials due to their remarkable characteristics of being a hydrogen bonding acceptor (O–H) and donor (C=O).[20,21] However, these MOFs have never been systematically investigated or intentionally designed for high-performance gas separation,[22–24] due to the significant coordination activity of carboxylic acids in MOF construction. We are interested in finely tuning MOFs to achieve efficient gas separations.[25–28] Herein, evolved from the interpenetrated **dia** topology,[29] a new family of 6-c MOFs (termed **NTU-71** to **NTU-73**) with carboxylic pincers were designed based upon a C_{2v} symmetric ligand of 3,5-di(1*H*-imidazol-1-yl)benzoic acid (**HL**) and the hybrid ions with different radii (SiF$_6$$^{2-}$ ($d_{Si–F}$: 1.690 Å), TiF$_6$$^{2-}$ ($d_{Ti–F}$: 1.886 Å) and ZrF$_6$$^{2-}$ ($d_{Zr–F}$: 1.983 Å)). Among them, the distance of their carboxylic pincers has been finely tailored, and thus, they may approach those found in crab-like systems (Scheme 1). Very interestingly, **NTU-72** exhibits a high C$_2$H$_2$/C$_2$H$_4$ selectivity and great ability for recovery of both highly pure C$_2$H$_4$ (99.95%) and C$_2$H$_2$ (99.36%). This excellent separation performance is due to the stabilization of a C$_2$H$_2$ tetramer by a couple of carboxylic pincers in the optimized pore geometry and size in **NTU-72**.
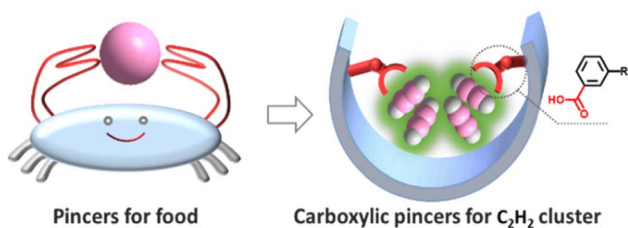
[a] State Key Laboratory of Materials-Oriented Chemical Engineering, Nanjing Tech University, Nanjing 211816, China. E-mail: duanjingui@njtech.edu.cn

[b] School of Chemistry and Molecular Engineering, Nanjing Tech University, Nanjing 211816, China. E-mail: bjunfeng@njtech.edu.cn

‡ These authors contributed equally to this work.

Scheme 1 Crab-inspired MOF design incorporating carboxylic pincers for selective recognition of a C_2H_2 cluster.

Experimental section

General procedures of the experiment and simulation are available in the ESI.†

Synthesis of NTU-70 to NTU-73

Synthesis of NTU-71. **HL** (4 mg, 0.015 mmol), $CuSiF_6$ (10 mg, 0.04 mmol) and H_2SiF_6 (100 μL) were mixed in DMA(dimethylacetamide)/H_2O/EtOH (1:1:1, 3 mL) in a 10 mL glass container and tightly capped with a Teflon vial and heated at 95 °C for 48 h. After cooling to room temperature, the resulting blue-green crystals were harvested and washed with fresh DMA three times. Yield is ∼49% (based on the ligand).

Synthesis of NTU-72. **HL** (4 mg, 0.015 mmol), $Cu(BF_4)_2$ (80 mg, 0.29 mmol), $(NH_4)_2TiF_6$(10 mg, 0.05 mmol) and H_2TiF_6 (100 μL) were mixed in DMA/H_2O/EtOH (1:1.5:1, 3.5 mL) in a 10 mL glass container and tightly capped with a Teflon vial and heated at 95 °C for 48 h. After cooling to room temperature, the resulting blue-green crystals were harvested and washed with fresh DMA three times. Yield is ∼53% (based on the ligand).

Synthesis of NTU-73. **HL** (4 mg, 0.015 mmol), $Cu(BF_4)_2$ (80 mg, 0.29 mmol), $(NH_4)_2ZrF_6$(10 mg, 0.04 mmol) and H_2ZrF_6 (100 μL) were mixed in DMA/H_2O/EtOH (1:1:1, 3 mL) in a 10 mL glass container and tightly capped with a Teflon vial and heated at 90 °C for 48 h. After cooling to room temperature, the resulting blue-green crystals were harvested and washed with fresh DMA three times. Yield is ∼32% (based on ligand).

Results and discussion

Synthesis and structure characterization

A reaction of copper(II) fluorosilicate with **HL** afforded polyhedron-shaped crystals (**NTU-71**). It crystallizes in a tetragonal $I4_122$ space group with the formula of $[Cu(\mathbf{HL})_2SiF_6]\cdot x$guest (Table S1†). Its asymmetric unit includes one ligand, half a Cu^{2+} ion and half a SiF_6^{2-} ion (Fig. S1†). The charge of all the Cu^{2+} ions in **NTU-71** is balanced by SiF_6^{2-} ions, and thus, all the **HL** ligands are neutral. The single Cu node here is coordinated by four imidazole nitrogen atoms from four independent **HL** and two F atoms from two SiF_6^{2-} anions. Meanwhile, the three general branching points of the ligand take part in the coordination with the Cu nodes by two imidazole N atoms, while the carboxylate sites are free. As a third component of this framework, two F atoms from the SiF_6^{2-} anion join the coordination of the adjacent Cu node, yielding two helical chains in this 3D framework (Fig. S2†). Obviously, two channels with densely incorporated carboxylic groups can be observed along the b- and c-axis (Fig. 1a and S3 and S4†). Like crab pincers, these carboxylate groups are packed in pairs throughout the whole
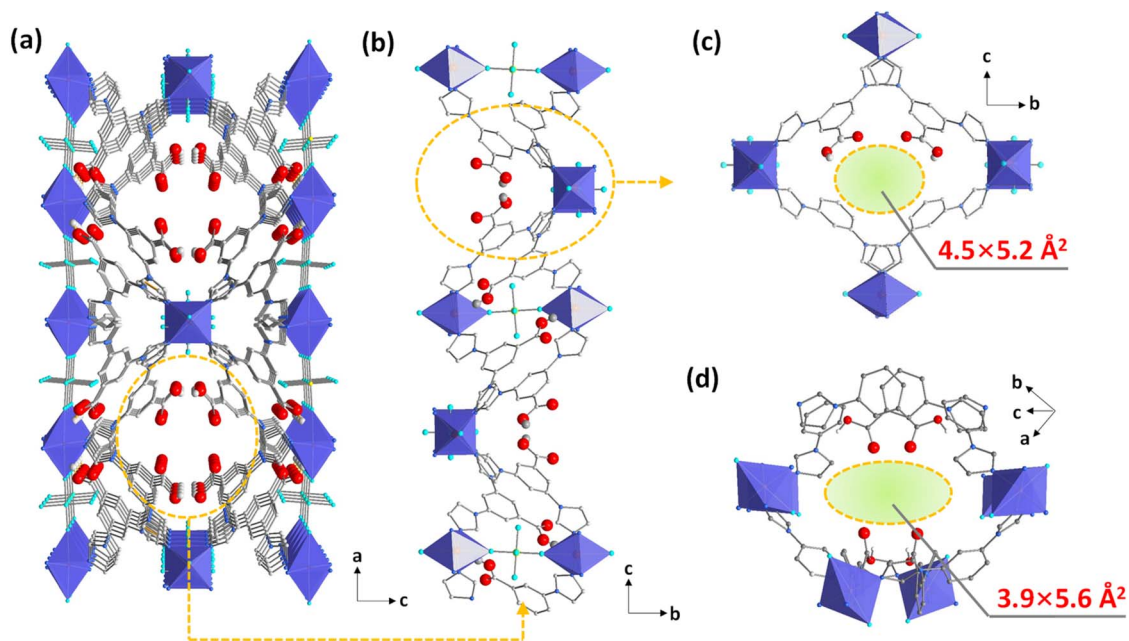

Fig. 1 Structure of **NTU-71**: view of the 1D channel that features carboxylic pincers along the b-axis (a); view of the pincers arranged alternately along the a-axis (b); local view of the nanospace defined by carboxylic pincers (c and d). Color codes: C, grey; N, blue; F, cyan; Si, yellow; O, red. The blue red polyhedron represents an octahedral coordinated Cu atom.

structure, and thus form a defined nanospace of about 4.5×5.2 Å^2 (Fig. 1b and c). In addition, these carboxylic pincers are also available in another semiregular channel with an aperture size of 3.9×5.6 Å^2 (Fig. 1d). To understand this structure better, topology analysis was performed. Cu(**HL**)$_2$ is an interpenetrated framework, of which each net can be simplified as a classical **dia** topology. Interestingly, these interpenetrated **dia** nets are then bridged by a 2-connected SiF$_6^{2-}$ anion, yielding a new 6-c topology with a point symbol of $\{4^8.6^7\}$ (Fig. S5†).

Nanospace tuning

Encouraged by this structure and reticular chemistry,[30] the fine pore size engineering of the carboxylic-functionalized MOFs was performed, in which the balancing SiF$_6^{2-}$ ions were replaced by TiF$_6^{2-}$ and ZrF$_6^{2-}$, respectively. With a general formula of [Cu(**HL**)$_2$MF$_6$], the other two iso-reticular MOFs (M = Ti^{2+} and Zr^{2+}, termed **NTU-72** and **NTU-73**) were obtained (Fig. S6–S8†). Compared with that of **NTU-71** ($d_{\text{O}\cdots\text{O}}$: 5.021 Å), the pincer distance increased to 5.583 Å and 5.911 Å in **NTU-72** and **NTU-73**, respectively (Fig. 2). These fine changes may offer a fitted nanospace for carboxylic pincers to recognize C$_2$H$_2$ clusters. The phase purity of these MOFs was examined by powder X-ray diffraction (PXRD). The diffraction peaks of the as-synthesized **NTU-series** are in good agreement with the simulated patterns, as well as the activated phases (Fig. S9–S11†).

Pore evaluation

Permanent porosity of **NTU-71** to **NTU-73** was further explored by N$_2$ (77 K) and CO$_2$ (195 K and 298 K) adsorption measurements. They all display negligible N$_2$ uptakes, but rapid and revisable type-I CO$_2$ adsorptions, indicating typical microporous characteristics. Their maximum CO$_2$ uptakes are 77, 82 and 71 cm^3 cm^{-3}, respectively (Fig. 3a). Their calculated BET surface areas (based on CO$_2$, 195 K) reach 242, 315 and 225 m^2 g^{-1}, respectively, while the analysis of pore size distributions illustrate the systematic change of the nanospace (inset of Fig. 3a).

Static adsorption selectivity and isosteric heats

Single-component adsorption isotherms of C$_2$H$_2$ and C$_2$H$_4$ were collected (Fig. 3b and S16–S21†), respectively. At 298 K, they all show relatively higher C$_2$H$_2$ uptakes compared with C$_2$H$_4$. Interestingly, the C$_2$H$_2$ uptakes (10.6 cm^3 g^{-1} and 8.2 cm^3 g^{-1}) at 1 kPa are almost 13–14 times higher than that of C$_2$H$_4$ (0.8 cm^3 g^{-1} and 0.6 cm^3 g^{-1}) in **NTU-71** and **NTU-73**, and this ratio (15.8 cm^3 g^{-1} *vs.* 1.0 cm^3 g^{-1}) increases to 16 in **NTU-72** (Fig. S22†). These higher uptake ratios reflect preferred affinity of the three frameworks toward C$_2$H$_2$ over C$_2$H$_4$. The adsorption selectivity of C$_2$H$_2$/C$_2$H$_4$ (v/v, 1/99) in these three MOFs was predicted by ideal adsorbed solution theory (IAST) (Fig. 3c and S23–S35†).[31,32] The low-pressure C$_2$H$_2$ adsorption selectivity of **NTU-72** ($\sim$441) is much higher than that of both **NTU-71** ($\sim$58) and **NTU-73** ($\sim$147), and is also higher than that of ZUL-200 (60),[33] NTU-69 (49),[34] SIFSIX-2-Cu-i (45),[7] and JCM-1 (9).[35] In addition, the C$_2$H$_2$ adsorption selectivities remain as high as 26, 56 and 38 at 1 bar. Particularly, the selectivity of **NTU-72** is only surpassed by the benchmark UTSA-200 (6320),[36] ZU-33 (1100),[37] and ZUL-series (175 and 114),[33] and is higher than most of the well known MOFs.[7,38]

To explore the reason for such high selectivities, isosteric heats of adsorption (Q_{st}) of C$_2$H$_2$ and C$_2$H$_4$ were calculated (Fig. 3d and S36–S41†). The Q_{st} values of C$_2$H$_4$ at low pressure (36.8, 36.7 and 35.7 kJ mol^{-1}) are all lower than that of C$_2$H$_2$ (42.4, 43.5, and 40.9 kJ mol^{-1}) for the **NTU-series**. Similar to the higher C$_2$H$_2$ uptake, the adsorption enthalpy difference of **NTU-72** (6.7 kJ mol^{-1}) is higher than that of **NTU-71** (5.6 kJ mol^{-1}) and **NTU-73** (5.2 kJ mol^{-1}). This may be due to the fine fitting of the pore geometry and size in **NTU-72** to the C$_2$H$_2$ molecule,
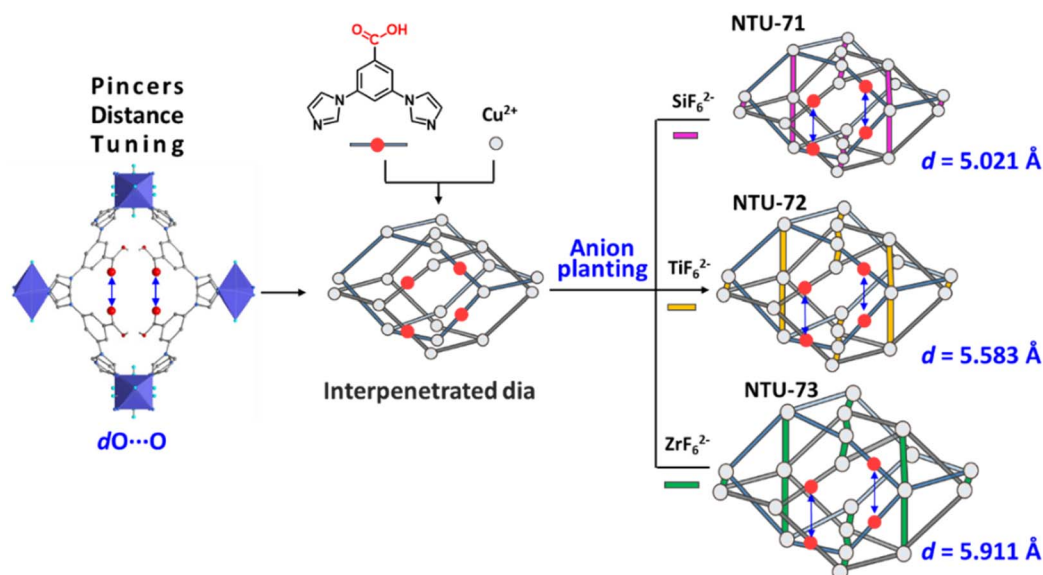

Fig. 2 Fine distance tuning in **NTU-series** *via* the anion planting approach, where $d_{\text{O}\cdots\text{O}}$ increases at the sub-angstrom level.
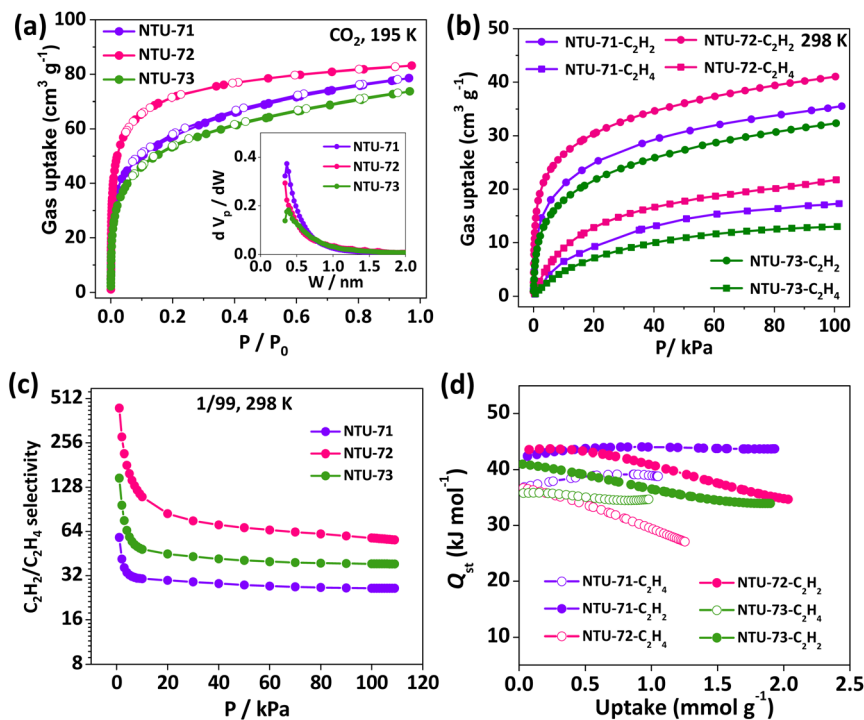
Fig. 3 Pore evaluation of the **NTU-series**: CO_2 adsorption isotherms (a), inset is the pore size distribution; C_2H_2 and C_2H_4 isotherms (b); IAST selectivity (c); isoteric heats (d).

while the relatively larger or smaller nanospace in **NTU-71** or **NTU-73** provides a small interaction difference.

Breakthrough experiments were performed on **NTU-72**, in which the binary mixtures of C_2H_2/C_2H_4 (v/v, 1/99) were introduced into the system. Pure C_2H_4 passed through the sample bed as the first component (4.2 min g^{-1}), while C_2H_2 is retained in the column (Fig. 4a). The mixtures of C_2H_2 and C_2H_4 were detected at about 71.1 min g^{-1}. This result shows that highly pure C_2H_4 (99.95%) can be directly collected in 66.9 min g^{-1} at the adsorption stage. According to the sample weight and gas velocity, **NTU-72** could produce 331.1 cm³ (STP) per g of pure C_2H_4 from this mixture. To confirm the selective adsorption, the saturated adsorbents were then swept by helium at 298 K until no signal was detected. Subsequently, C_2H_2 was desorbed by rapid heating (up to 323 K), and its purity is approximately 99.36% (Fig. 4b and S42 and S43†). Therefore, as an emerging example, **NTU-72** can deliver both highly pure C_2H_4 and C_2H_2 in one adsorption/desorption cycle, although the recovery of poly-grade C_2H_4 has been widely reported (Table S2†). Structural stability was then confirmed by cycling breakthrough experiments, where nearly the same separation curves were displayed (Fig. 4c). Further experiments with varied gas velocity (2 and 10 cm³ min⁻¹) also showed obvious separation, and the C_2H_4 productivity (319.6 and 323.8 cm³ (STP) per g) has hardly suffered any impact (Fig. 4d and S44†).

To gain better understanding of the separation performance, C_2H_2- and C_2H_4-loaded **NTU-72** crystals were investigated at 298 K.[39] As expected, both gases interact with the carboxylic sites (Fig. S45 and S46†). For **NTU-72**⊃C_2H_2, the occupancy of C_2H_2 was refined to be 1, which corresponds to 30.5 cm³ g^{-1}, slightly

lower than the amount in the C_2H_2 adsorption experiment (41 cm³ g^{-1}) at 1 bar. This difference may be caused by two reasons: (1) the C_2H_2 molecules at other free space are strongly disordered and hard to be accurately modelled; (2) part of the C_2H_2 escaped during the sealing of the glass tube by using a hot candle. Despite this, the position and geometry of the adsorbed C_2H_2 molecules can be clearly identified in this confined nanospace. The C_2H_2 molecules are confined in the channel through three types of hydrogen bonds in different binding geometries (Fig. 5a and b). Acting as an acceptor and a donor, the O_{COOH} and OH_{COOH} moieties connect the terminal hydrogen and carbon atoms of a C_2H_2 molecule. In addition, the OH_{COOH} moiety also forms a hydrogen bond with another C_2H_2 molecule, resulting in close packing of the two gas molecules with intermolecular hydrogen bonds. Meanwhile, the terminal H_{C2H2} forms hydrogen bonds with C_{C2H2} from its symmetrically equivalent molecule, so that a C_2H_2 tetramer with C_{2h} symmetry is formed periodically in **NTU-72** (Fig. S47–S49†), which is different from the S_4 symmetric C_2H_2 tetramer in SIFSIX-Cu-i.[7] Although the C_2H_2 clusters have been investigated,[20,21] a compact C_2H_2 tetramer with C_{2h} symmetry being stabilized by chelating carboxylic pincers is found for the first time. Sharply in contrast, two types of hydrogen bonds are observed in **NTU-72**⊃C_2H_4 (Fig. 5c and d and S50–S52†). Particularly, $d_{C2H4}\cdots H-O_{COOH}$ (2.705 Å) is much longer than that of $d_{C2H2}\cdots H-O_{COOH}$ (1.871 and 2.588 Å), as well as the longer $d_{O_{COOH}}\cdots H-O_{C2H4}$, reflecting relative weak carboxylic–C_2H_4 interaction. Furthermore, no intermolecular interaction is found between the two C_2H_4 molecules, as their distance is far. Therefore, the carboxylic sites contribute mainly to the
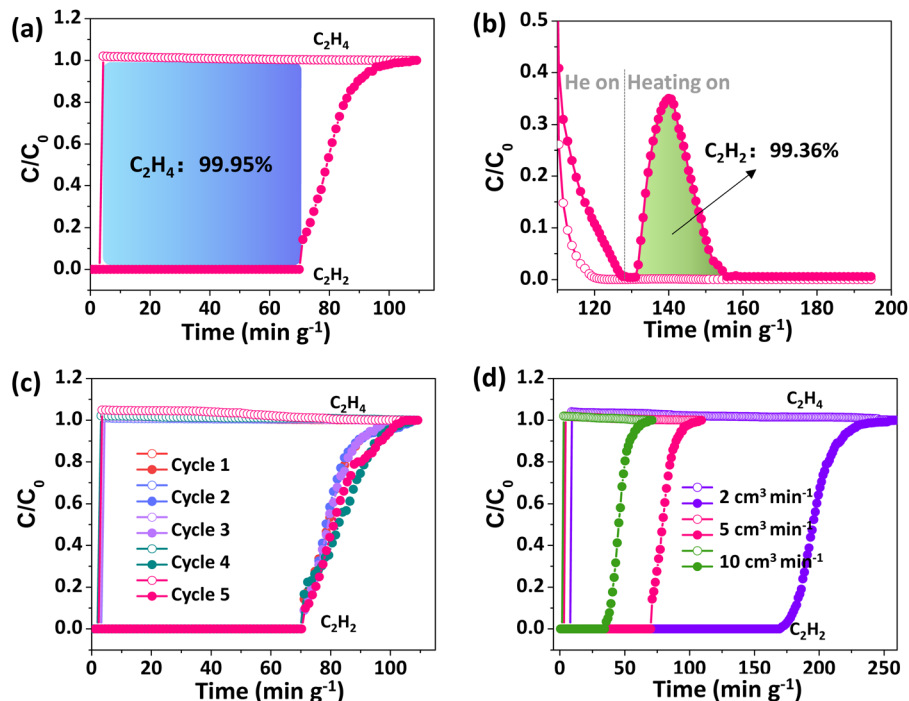
Fig. 4 Breakthrough curves of **NTU-72** for a C_2H_2/C_2H_4 mixture (1/99, v/v) at 298 K, 1 bar, velocity is 5 cm^3 min^{-1} (a); desorption curves (b); cycle breakthrough tests (c); (d) breakthrough curves at different velocities.

recognition of the C_2H_2 tetramer, and meanwhile, the finely engineered pore geometry and nano-size confined this cluster to be released in the pure form. Further Raman spectra of gas loaded **NTU-72** show that the peak at 1950 cm^{-1} belonging to the tensile vibration of C_2H_2 was found in **NTU-72**, and in contrast, no helium peak was found (Fig. 5e).[40,41] In addition,

the corresponding peak that belongs to C_2H_4 (theoretical position: 1689 cm^{-1}) can't be observed. Therefore, it is rational to conclude that the C_2H_2 clusters assembled in a periodic configuration in **NTU-72**, agreeing well with the crystallographic studies.
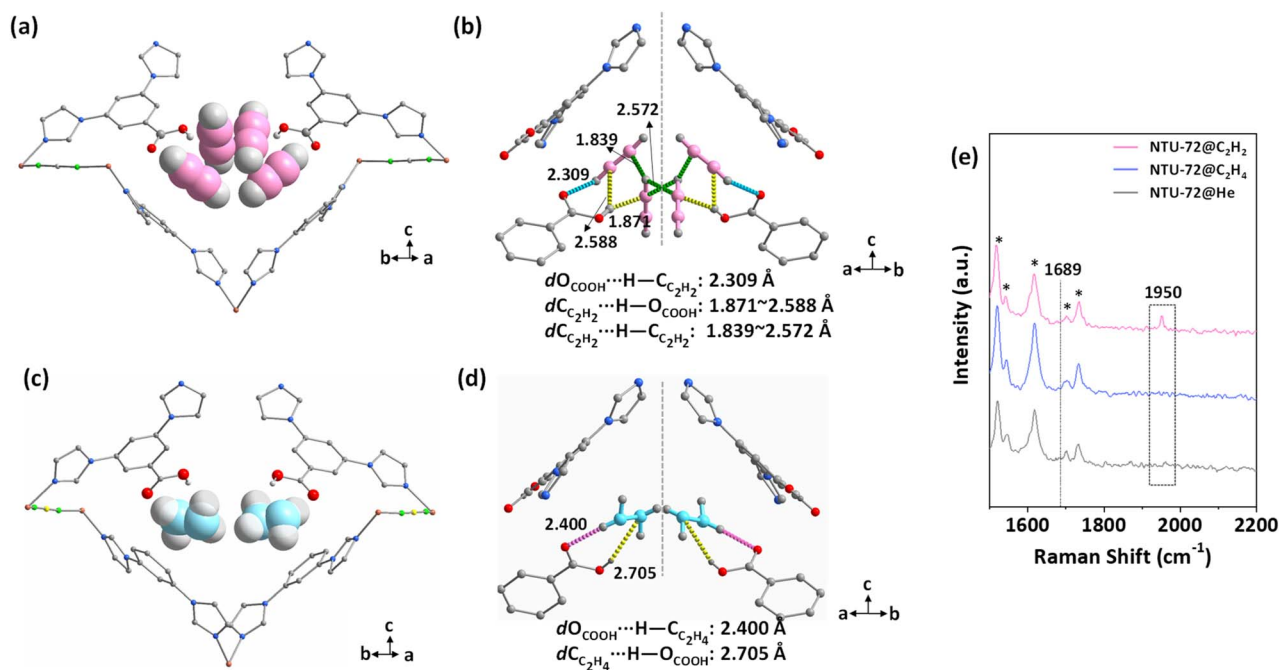

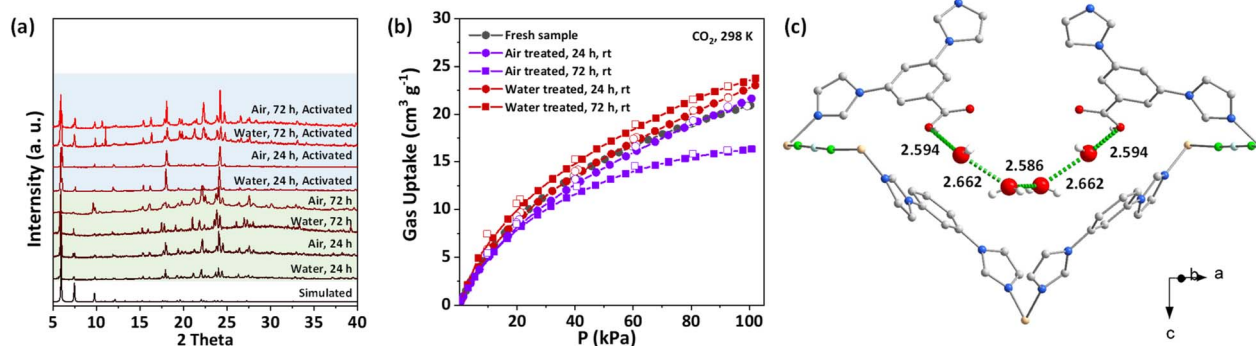**Fig. 5** Structure of C_2H_2- (a and b) and C_2H_4- (c and d) loaded **NTU-72**. Raman spectra of gas-loaded **NTU-72** (e).

Fig. 6 PXRD (a) and CO_2 adsorption isotherms (b) of water and moisture treated **NTU-72**; local view of the structure of **NTU-72$\supset$H$_2$O** (c), and the unit of O⋯O distance is Å.

Stability

The water/air stability of **NTU-72** was then evaluated at room temperature. As shown in Fig. S53,† **NTU-72** retained a polyhedral shape after air treatment, but some changes occurred in the shape after water treatment. Single crystal X-ray analysis showed that the water treated crystal (**NTU-72$\supset$H$_2$O**, for 72 h) retains the framework of the as-synthesized phase (Table S1†), confirmed further by PXRD analysis. Additionally, adsorption measurements revealed that the CO_2 capacity of all treated samples is consistent with that of fresh samples, except for a slight decrease in the air treated sample for 72 h. These results confirm that **NTU-72** has good water and moisture robustness (Fig. 6a and b). Considering the structure, the maintained crystallinity of **NTU-72** is due to the relatively strong Cu–N bond, similar to that of **NTU-67**, having a highly robust framework with a Cu–N coordination sphere also.[39] In addition, the crystal structure of **NTU-72$\supset$H$_2$O** shows that a couple of carboxylic pincers bind a tetra-water cluster via short hydrogen bonds ($d_{O\cdots O}$: 2.586–2.662 Å), which may provide a blocking effect for other water molecules to reach the coordination bonds (Fig. 6c).

Conclusions

In conclusion, as needed for the pure C2 hydrocarbons, we have finely tuned a new family of carboxylic-functionalized MOFs and afforded **NTU-72** with high adsorption C_2H_2/C_2H_4 selectivity as well as unprecedented recovery of highly pure C_2H_4 and C_2H_2. The carboxylic pincers contribute to the recognition of a C_2H_2 tetramer, and the fitted pore geometry/size enforces synergistic binding and restricts this cluster to be released in a pure form. In addition, this material is stable in water and moisture environments. The foregoing results not only present an excellent MOF for energy-saving C2 hydrocarbon purification, but also provide a novel approach for the selective binding of gas clusters for designing advanced MOFs.

Data availability

All data can be found in the main text and ESI.†

Author contributions

J. D. conceived the idea of this work. Y. D. and Y. H. carried out the experiments and analyzed the results. J. D. and J. B. wrote the paper. C. W. performed the repeated adsorption experiments. H. W. prepared the ligands. All authors gave valuable discussion and suggestion for the final draft.

Conflicts of interest

The authors declare no competing interests.

Acknowledgements

References

1 D. S. Sholl and R. P. Lively, *Nature*, 2016, **532**, 435–437.

2 R. Matsuda, R. Kitaura, S. Kitagawa, Y. Kubota, R. V. Belosludov, T. C. Kobayashi, H. Sakamoto, M. Takata, Y. Kawazoe and Y. Mita, *Nature*, 2005, **436**, 238–241.

3 Y. Chai, X. Han, W. Li, S. Liu, S. Yao, C. Wang, W. Shi, I. da-Silva, P. Manuel, Y. Cheng, L. D. Daemen, A. J. Ramirez-Cuesta, C. C. Tang, L. Jiang, S. Yang, N. Guan and L. Li, *Science*, 2020, **368**, 1002–1006.

4 K. J. Chen, D. G. Madden, S. Mukherjee, T. Pham, K. A. Forrest, A. Kumar, B. Space, J. Kong, Q. Y. Zhang and M. J. Zaworotko, *Science*, 2019, **366**, 241–246.

5 F. Studt, F. Abild-Pedersen, T. Bligaard, R. Z. Sorensen, C. H. Christensen and J. K. Norskov, *Science*, 2008, **320**, 1320–1322.

6 E. D. Bloch, W. L. Queen, R. Krishna, J. M. Zadrozny, C. M. Brown and J. R. Long, *Science*, 2012, **335**, 1606–1610.

7 X. L. Cui, K. J. Chen, H. B. Xing, Q. W. Yang, R. Krishna, Z. B. Bao, H. Wu, W. Zhou, X. L. Dong, Y. Han, B. Li, Q. L. Ren, M. J. Zaworotko and B. L. Chen, *Science*, 2016, **353**, 141–144.

8 B. Li, X. Cui, D. O'Nolan, H. M. Wen, M. Jiang, R. Krishna, H. Wu, R. B. Lin, Y. S. Chen, D. Yuan, H. Xing, W. Zhou, Q. Ren, G. Qian, M. J. Zaworotko and B. Chen, *Adv. Mater.*, 2017, **29**, 1704210–1704217.

9 H. Zeng, M. Xie, T. Wang, R. J. Wei, X. J. Xie, Y. F. Zhao, W. G. Lu and D. Li, *Nature*, 2021, **595**, 542–548.

10 A. Cadiau, K. Adil, P. M. Bhatt, Y. Belmabkhout and M. Eddaoudi, *Science*, 2016, **353**, 137–140.

11 Q. Dong, Y. Huang, J. Wan, Z. Lu, Z. Wang, C. Gu, J. Duan and J. Bai, *J. Am. Chem. Soc.*, 2023, DOI: 10.1021/jacs.3c00515.

12 H. Li, M. Eddaoudi, M. O'Keeffe and O. M. Yaghi, *Nature*, 1999, **402**, 276–279.

13 S. Krause, V. Bon, I. Senkovska, U. Stoeck, D. Wallacher, D. M. Tobbens, S. Zander, R. S. Pillai, G. Maurin, F. X. Coudert and S. Kaskel, *Nature*, 2016, **532**, 348–352.

14 S. H. Lo, L. Feng, K. Tan, Z. H. Huang, S. Yuan, K. Y. Wang, B. H. Li, W. L. Liu, G. S. Day, S. S. Tao, C. C. Yang, T. T. Luo, C. H. Lin, S. L. Wang, S. J. L. Billinge, K. L. Lu, Y. J. Chabal, X. D. Zou and H. C. Zhou, *Nat. Chem.*, 2020, **12**, 90–97.

15 H. Wang, X. L. Dong, V. Colombo, Q. N. Wang, Y. Y. Liu, W. Liu, X. L. Wang, X. Y. Huang, D. M. Proserpio, A. Sironi, Y. Han and J. Li, *Adv. Mater.*, 2018, **30**, 1805088–1805096.

16 Y. L. Peng, T. Pham, P. Li, T. Wang, Y. Chen, K. J. Chen, K. A. Forrest, B. Space, P. Cheng, M. J. Zaworotko and Z. Zhang, *Angew. Chem., Int. Ed.*, 2018, **57**, 10971–10975.

17 R. B. Lin, L. B. Li, H. Wu, H. Arman, B. Li, R. G. Lin, W. Zhou and B. L. Chen, *J. Am. Chem. Soc.*, 2017, **139**, 8022–8028.

18 J. P. Zhang, P. Q. Liao, H. L. Zhou, R. B. Lin and X. M. Chen, *Chem. Soc. Rev.*, 2014, **43**, 5789–5814.

19 N. Behera, J. Duan, W. Jin and S. Kitagawa, *EnergyChem*, 2021, **3**, 100067–100124.

20 K. Shuler and C. E. Dykstra, *J. Phys. Chem. A*, 2000, **104**, 11522–11530.

21 J. G. Yu, S. J. Su and J. E. Bloor, *J. Phys. Chem.*, 1990, **94**, 5589–5592.

22 R. Custelcean and M. G. Gorbunova, *J. Am. Chem. Soc.*, 2005, **127**, 16362–16363.

23 X. Duan, R. J. Song, J. C. Yu, H. L. Wang, Y. J. Cui, Y. Yang, B. L. Chen and G. D. Qian, *RSC Adv.*, 2014, **4**, 36419–36424.

24 F. Ragon, B. Campo, Q. Yang, C. Martineau, A. D. Wiersum, A. Lago, V. Guillerm, C. Hemsley, J. F. Eubank, M. Vishnuvarthan, F. Taulelle, P. Horcajada, A. Vimont, P. L. Llewellyn, M. Daturi, S. Devautour-Vinot, G. Maurin, C. Serre, T. Devic and G. Clet, *J. Mater. Chem. A*, 2015, **3**, 3294–3309.

25 J. Duan, M. Higuchi, J. Zheng, S. I. Noro, I. Y. Chang, K. Hyeon-Deuk, S. Mathew, S. Kusaka, E. Sivaniah, R. Matsuda, S. Sakaki and S. Kitagawa, *J. Am. Chem. Soc.*, 2017, **139**, 11576–11583.

26 Z. Y. Lu, L. T. Du, R. Y. Guo, G. B. Zhang, J. G. Duan, J. F. Zhang, L. Han, J. F. Bai and J. T. Hupp, *J. Am. Chem. Soc.*, 2021, **143**, 17942–17946.

27 M. X. Zhang, W. Zhou, T. Pham, K. A. Forrest, W. L. Liu, Y. B. He, H. Wu, T. Yildirim, B. L. Chen, B. Space, Y. Pan, M. J. Zaworotko and J. F. Bai, *Angew. Chem., Int. Ed.*, 2017, **56**, 11426–11430.

28 L. Du, Z. Lu, K. Zheng, J. Wang, X. Zheng, Y. Pan, X. You and J. Bai, *J. Am. Chem. Soc.*, 2013, **135**, 562–565.

29 M. Li, D. Li, M. O'Keeffe and O. M. Yaghi, *Chem. Rev.*, 2014, **114**, 1343–1370.

30 N. W. Ockwig, O. Delgado-Friedrichs, M. O'Keeffe and O. M. Yaghi, *Acc. Chem. Res.*, 2005, **38**, 176–182.

31 J. G. Duan, M. Higuchi, S. Horike, M. L. Foo, K. P. Rao, Y. Inubushi, T. Fukushima and S. Kitagawa, *Adv. Funct. Mater.*, 2013, **23**, 3525–3530.

32 R. Krishna, *RSC Adv.*, 2015, **5**, 52269–52295.

33 J. Shen, X. He, T. Ke, R. Krishna, J. M. van Baten, R. Chen, Z. Bao, H. Xing, M. Dinca, Z. Zhang, Q. Yang and Q. Ren, *Nat. Commun.*, 2020, **11**, 6259.

34 Y. Huang, Y. Xu, B. Zheng, Z. Wang, Q. Dong and J. Duan, *Energy Fuels*, 2020, **34**, 11315–11321.

35 J. Lee, C. Y. Chuah, J. Kim, Y. Kim, N. Ko, Y. Seo, K. Kim, T. H. Bae and E. Lee, *Angew. Chem., Int. Ed.*, 2018, **57**, 7869–7873.

36 H. Li, L. Li, R. B. Lin, G. Ramirez, W. Zhou, R. Krishna, Z. Zhang, S. Xiang and B. Chen, *ACS Sustainable Chem. Eng.*, 2019, **7**, 4897–4902.

37 Z. Zhang, X. Cui, L. Yang, J. Cui, Z. Bao, Q. Yang and H. Xing, *Ind. Eng. Chem. Res.*, 2018, **57**, 7266–7274.

38 J. Wang, L. Li, L. Guo, Y. Zhao, D. Xie, Z. Zhang, Q. Yang, Y. Yang, Z. Bao and Q. Ren, *Chem.–Eur. J.*, 2019, **25**, 15516–15524.

39 Q. B. Dong, Y. H. Huang, K. Hyeon-Deuk, I. Y. Chang, J. M. Wan, C. L. Chen, J. G. Duan, W. N. Jin and S. Kitagawa, *Adv. Funct. Mater.*, 2022, **32**, 2203745–2203755.

40 H. Wang, Y. Duan, Y. Wang, Y. Huang, K. Ge, S. Wang, B. Zheng, Z. Wang, J. Bai and J. Duan, *ACS Appl. Mater. Interfaces*, 2022, **14**, 13550–13559.

41 G. C. Guo, S. H. Lin, F. K. Zheng, Z. C. Dong and J. S. Huang, *Spectrosc. Spectral Anal.*, 2000, **20**, 830–832.